Identifying the perfect absorption of metamaterial absorbers

G. Duan,[1] J. Schalch,[2] X. Zhao,[1] J. Zhang,[2] R. D. Averitt,[2,*] and X. Zhang[1,†]
[1]*Department of Mechanical Engineering, Boston University, Boston, Massachusetts 02215, USA*
[2]*Department of Physics, University of California, San Diego, La Jolla, California 92093, USA*

(Received 31 July 2017; revised manuscript received 7 December 2017; published 16 January 2018)

We present a detailed analysis of the conditions that result in unity absorption in metamaterial absorbers to guide the design and optimization of this important class of functional electromagnetic composites. Multilayer absorbers consisting of a metamaterial layer, dielectric spacer, and ground plane are specifically considered. Using interference theory, the dielectric spacer thickness and resonant frequency for unity absorption can be numerically determined from the functional dependence of the relative phase shift of the total reflection. Further, using transmission line theory in combination with interference theory we obtain analytical expressions for the unity absorption resonance frequency and corresponding spacer layer thickness in terms of the bare resonant frequency of the metamaterial layer and metallic and dielectric losses within the absorber structure. These simple expressions reveal a redshift of the unity absorption frequency with increasing loss that, in turn, necessitates an increase in the thickness of the dielectric spacer. The results of our analysis are experimentally confirmed by performing reflection-based terahertz time-domain spectroscopy on fabricated absorber structures covering a range of dielectric spacer thicknesses with careful control of the loss accomplished through water absorption in a semiporous polyimide dielectric spacer. Our findings can be widely applied to guide the design and optimization of the metamaterial absorbers and sensors.

DOI: 10.1103/PhysRevB.97.035128

I. INTRODUCTION

Absorbers have been investigated across the electromagnetic spectrum from microwave to optical region [1–4]. The traditional absorber at microwave frequencies is the circuit-analog absorber, usually configured with quarter wavelength thickness with a carefully selected resistivity for the high-impedance surface, and the applications are limited within the microwave range [5–7]. To overcome these limitations, metamaterial absorbers were proposed and widely studied as three-layer configurations consisting of a dielectric spacer separating two additional layers that are often composed of metals [1,2,8]. Usually one (or both) of the separated layers is a metasurface designed with a resonance frequency dictated by the subwavelength geometry and local dielectric environment [9–12]. In an absorber configuration at resonance, incident electromagnetic radiation is effectively trapped between the two separated layers and is absorbed in the dielectric and metallic regions, ultimately being dissipated entirely as heat. Although this intuitive explanation is straightforward, theoretical analysis of the nature of unity absorption is important to gain quantitative insights into the underlying physics. Various theories and models have been utilized to advance the understanding of perfect absorption [2,13–17]. For example, in Ref. [18] coupled-mode theory provides a detailed description of unity absorption in terms of absorptive and radiative losses. However, it is important to develop alternative numerical and analytical strategies that transparently connect with the electromagnetic and dielectric properties of the constituent materials to better understand how experimentally accessible parameters ultimately determine the absorption.

We analyze the conditions resulting in perfect absorption in metamaterials by employing inference theory and transmission line theory. Our results show that the dielectric spacer thickness and frequency for unity absorption can be numerically obtained from the relative phase shift of the total reflection. Additional analysis using transmission line theory reveals that the critical spacer thickness for unity absorption is correlated with the system loss. The results are experimentally verified by employing semiporous polyimide as the dielectric spacer. Our analysis offers new insights toward a more complete understanding of metamaterial perfect absorbers and can be generally applied to guide the design and optimization of arbitrary absorber geometries.

II. INTERFERENCE THEORY AND PERFECT ABSORPTION

A. Absorber design and interference theory

Without loss of generality, a terahertz (THz) metamaterial absorber composed of an array of split ring resonators (SRRs), a dielectric spacer, and a ground plane was employed as a testbed for the ensuing analysis. The SRR geometry is shown as the inset in Fig. 1(a). The periodicity of the array was 45 μm and the permittivity of the spacer material was taken as $2.81 \times (1 + 0.03i)$ for cured polyimide (PI-5878G). The reflection and transmission characteristics of the MMs on top of the spacer in the absence of a ground plane were simulated using the CST microwave studio frequency domain solver with periodic boundary conditions. Gold was modeled as lossy metal with conductivity of 4.56×10^7 S/m. The complex

*raveritt@ucsd.edu
†xinz@bu.edu

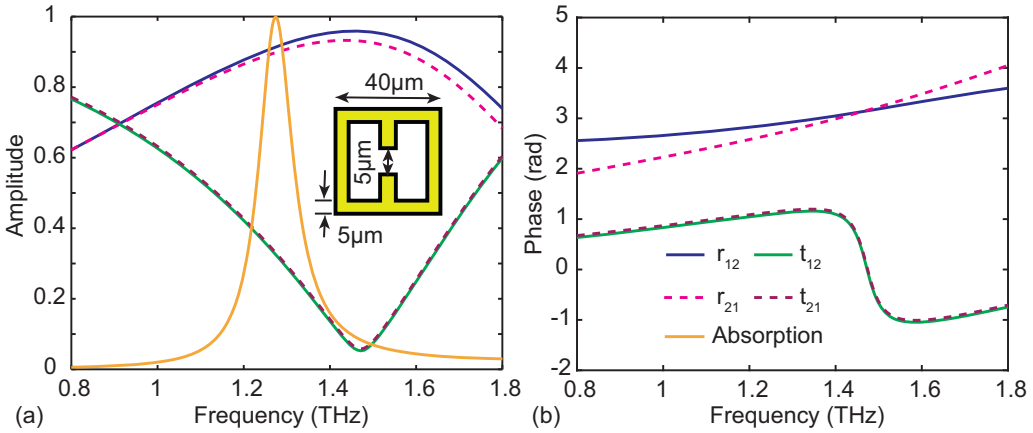

FIG. 1. The retrieved reflection and transmission parameters from simulation. (a) Amplitude spectra and (b) phase spectra. The inset shows the geometry of the SRR unit cell with period of 45 μm for the array. The perfect absorption spectrum is plotted in (a) for a spacer thickness of 5 μm.

reflection (r_{12}) and transmission (t_{12}) coefficients (for the air-SRR array interface) and r_{21} and t_{21} (for the spacer-SRR array interface) determined from the simulations are plotted in Fig. 1. According to interference theory the overall reflection of the metamaterial absorber with spacer thickness of d can be considered as the interference between the multiple reflections and is expressed as [19,20]

$$r = r_{12} - \frac{t_{12}t_{21}}{r_{21} + e^{-i2\beta}}, \tag{1}$$

where r is the total reflection, $\beta = nkd$ is the one-way phase delay in the spacer, and n, k are the refractive index of the spacer material and the wave number in vacuum, respectively. In the remainder of this manuscript, we denote r_{12} as the first reflection and $-t_{12}t_{21}/(r_{21} + e^{-i2\beta})$ as the secondary reflection with the absorption expressed as $A = 1 - |r|^2$ (due to zero transmission because of the ground plane). As is well known, to subsequently obtain a perfect absorber with the metamaterial structure and spacer material described above, the correct spacer layer thickness for the spacing between the SRR array and a metallic ground plane must be utilized. For a spacer thickness of 5 μm, the gold line in Fig. 1(a) results in unity absorption. The design process for perfect absorption will be explained in detail in the following paragraphs.

B. Phase shift and perfect absorption

In Eq. (1), the overall reflection is directly related to the spacer thickness, which governs the amplitude and phase of the secondary reflection. When the secondary reflection and the first reflection are antiphased and of the same amplitude for a critical spacer thickness, there will be complete destructive interference, leading to perfect absorption. In this paper, we are only considering the "metamaterial regime," corresponding to the thinnest spacer layer that results in perfect absorption. The phase and amplitude of the first reflection and the secondary reflection for different spacer thicknesses are plotted in Figs. 2(a) and 2(b), along with labeled absorption peak frequencies. From the phase spectra [Fig. 2(a)], it is evident that the phase difference between the first and secondary reflection approaches π at the absorption peak frequencies (highlighted with circles). At the critical spacer thickness of $d = 5\,\mu$m the phase shift is almost exactly π as required for perfect absorption. Moreover, as the spacer thickness increases, the amplitude of the secondary reflection [Fig. 2(b)] increases and gradually becomes larger than the amplitude of the first reflection. As expected, where the amplitudes are equal [Fig. 2(b)] and the phase shift is π, perfect absorption results.

Of particular importance is the dramatic evolution of the overall phase shift spectrum for spacer thicknesses close to the critical thickness. As shown in Fig. 2(c), at and beyond the critical spacer thickness the phase can cover a full 2π. This makes it possible to pinpoint the perfect absorption point based on the phase shift diagram of the total reflection. Figure 2(d) depicts the phase shift diagram of the overall reflection versus frequency and spacer thickness. When the spacer thickness is thinner than the critical spacer thickness value, the phase coverage of the total reflection is smaller than π. However, when it is thicker than the critical value, the phase of the overall reflection is able to extend beyond zero and cover the entire 2π range due to the increasing effect of the secondary reflection. The critical point is the point at which perfect absorption can be achieved and can be visually identified on the phase diagram as 5 μm for the spacer thickness and as 1.28 THz for the frequency in this example. Importantly, although the results of the analysis carried out above apply to the specific metamaterial structure model utilized, the phase shift diagram can, in principle, be employed to pinpoint the spacer thickness and the corresponding frequency for perfect absorption for any other metamaterial structures using their unique reflection and transmission coefficients. In the following, we first verify these results experimentally, and then obtain analytical expressions for the perfect absorption spacer thickness and frequency in terms of the properties of the SRRs and the dielectric function of the spacer layer.

C. Experimental validation

Metamaterial absorbers with unit cell structure and geometries illustrated in the inset of Fig. 1(a) (i.e., with the parameters used in the simulations above) were fabricated with different spacer thicknesses by employing polyimide (PI-5878G) as the spacer material. The thickness of the spacer was

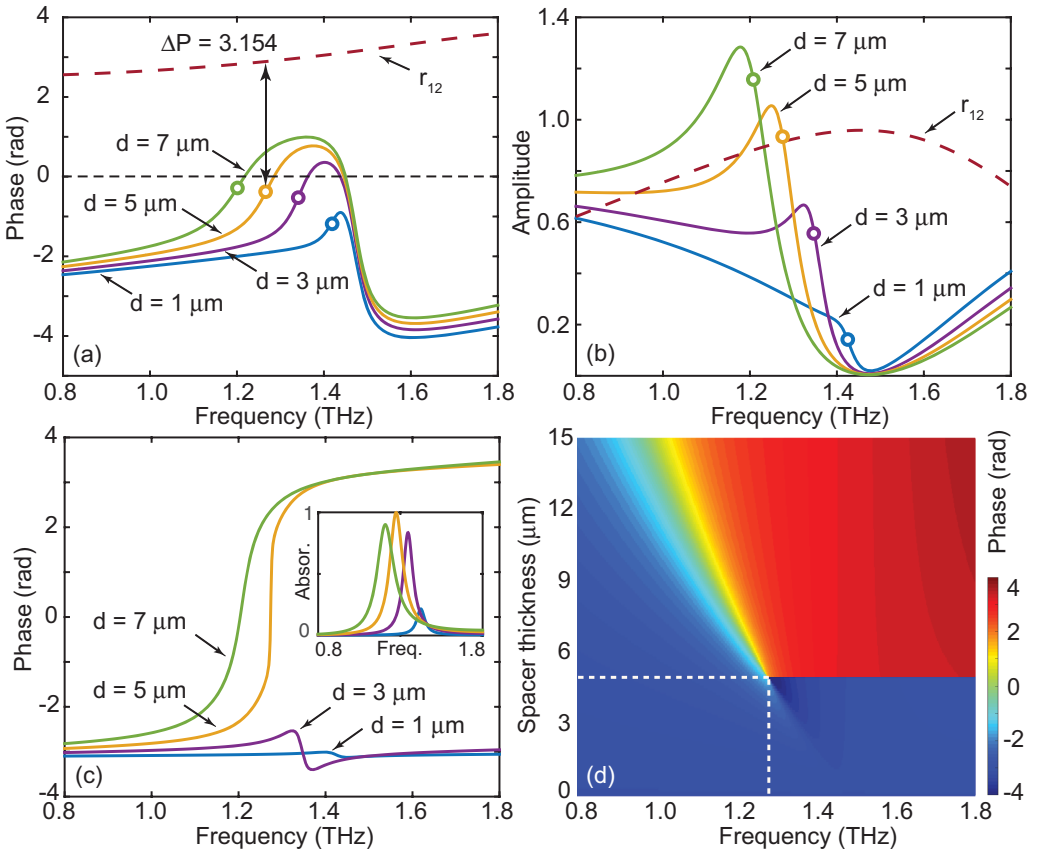

FIG. 2. The (a) phase and (b) amplitude spectra of the first (dashed line) and secondary reflection (solid lines) with different spacer thicknesses. The absorption peak frequency points are labeled with circles. (c) Phase spectra of the total reflection for different spacer thicknesses with the inset showing the corresponding absorption. (d) Color plot of the calculated total phase shift as a function of frequency and spacer thickness. The white dashed lines show the spacer thickness (5 μm) and the corresponding frequency (1.28 THz) for the perfect absorption.

measured as 3.8, 5.3, and 6.0 μm using surface profilometry. Subsequently, the samples were characterized with THz time domain spectroscopy (THz-TDS). The measured absorption and phase spectra are depicted in Fig. 3 (solid lines) with simulated spectra as comparison (dashed lines). The insets in Figs. 3(a) and 3(b) show the image of a fabricated sample and the unit cell structure. The evolution of the phase spectra is clearly revealed, with the critical spacer thickness of 5.3 μm having near-unity absorption with an abrupt phase shift of 2π in the vicinity of the perfect absorption frequency. With the basic description of the perfect absorption phenomena and experimental verification of the phase shift at the critical spacer thickness, we now present a derivation of equations to gain additional insight into metamaterial perfect absorbers.

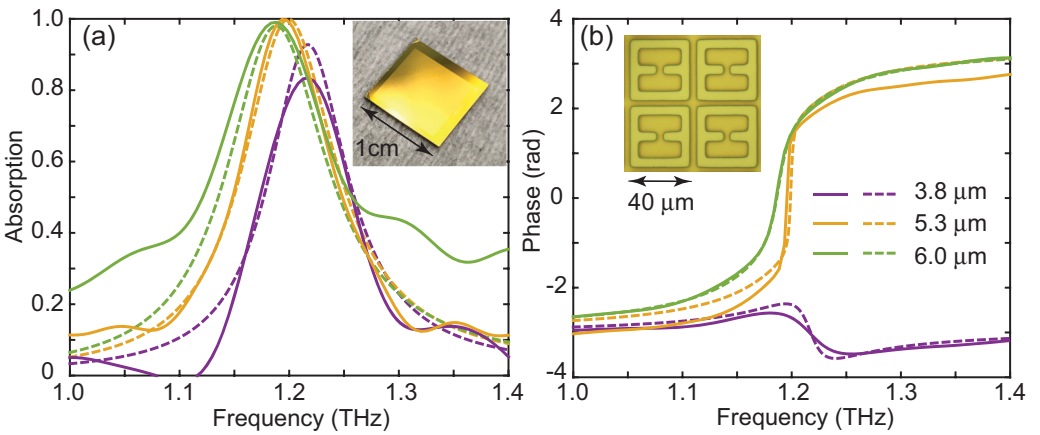

FIG. 3. Experiment (solid lines) and simulation (dashed lines). (a) Absorption spectra and (b) total reflection phase spectra for metamaterial absorbers with different spacer thicknesses of 3.8, 5.3, and 6.0 μm. The insets in (a) and (b) show the image of a fabricated sample and the unit cell structure.

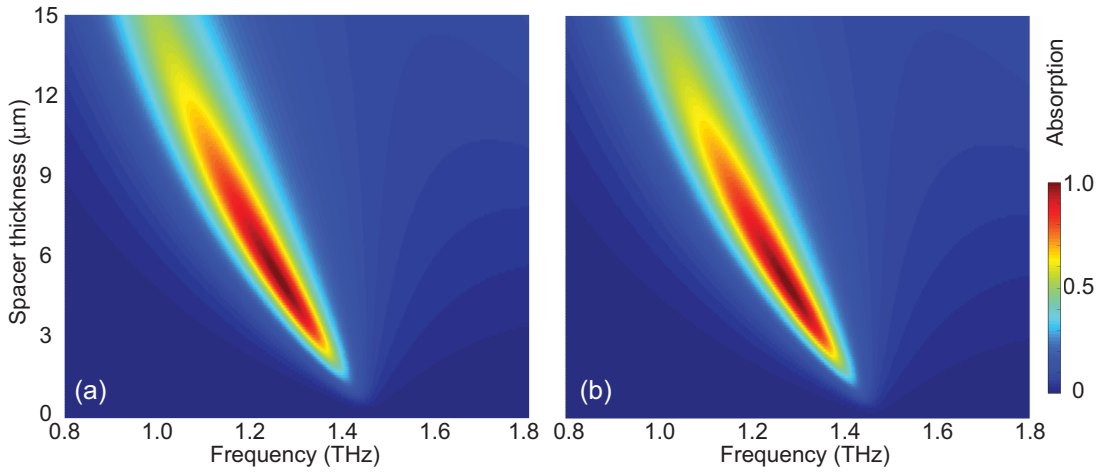

FIG. 4. Absorption diagram based on the reflection and transmission parameters retrieved from (a) transmission line model and (b) simulation.

III. MATERIAL DEPENDENCE AND PERFECT ABSORPTION

A. Transmission line model

To analytically locate the frequency and the spacer thickness to achieve perfect absorption, transmission line theory is used to model the SRRs and calculate the reflection and transmission coefficients (r_{12}, t_{12}, r_{21}, and t_{21}) analytically. SRRs can be modeled as having LC and dipole resonant modes connected in parallel [21]. Further, the impedance of each mode can be expressed as series RLC resonators given as [22]

$$Z_{\mathrm{LC,dipole}} = R_{\mathrm{LC,dipole}} + \frac{2\varepsilon_i}{\omega C_{\mathrm{LC,dipole}}(\varepsilon_r+1)^2} + j\omega L_{\mathrm{LC,dipole}} + \frac{2}{j\omega C_{\mathrm{LC,dipole}}(\varepsilon_r+1)}, \quad (2)$$

where ε_r and ε_i are the real part and imaginary part of the spacer permittivity. Z_{LC} and Z_{dipole} are the impedance of the LC and dipole modes, respectively, and $R_{\mathrm{LC,dipole}}$, $L_{\mathrm{LC,dipole}}$, and $C_{\mathrm{LC,dipole}}$ are the fitted resistance, inductance, and capacitance value for the free standing SRRs (applies to only the metallic structure *without* spacer material), respectively. On the right-hand side of the equation, the first term represents the metallic loss contributed by the joule heating in the SRRs. The second term represents the dielectric loss of the spacer layer and the third and the forth terms are the reactance from the equivalent inductance and capacitance of the SRRs. The Supplemental Material [23] provides details of the fitting to obtain the effective circuit parameters. To simplify the analysis, the coupling between the two modes was neglected and, therefore, the impedance of the MMs can be calculated as

$$Z_m = \frac{Z_{\mathrm{LC}} \cdot Z_{\mathrm{dipole}}}{Z_{\mathrm{LC}} + Z_{\mathrm{dipole}}}. \quad (3)$$

The impedance values of free space (Z_0) and the spacer material (Z_{d}) were set as the impedance values of the input port and output port, respectively, and can be connected by

$$Z_d = k_m Z_0, \quad (4)$$

where k_m equals to $\sqrt{1/(\varepsilon_r - i\varepsilon_i)}$ [24]. The ABCD parameters can be calculated by assuming the transmission line is shunt connected by the impedance of the MMs and converted to S parameters [25]. Considering that the reference direction is negative, the reflection and transmission parameters are the conjugate of the S parameters as

$$\begin{bmatrix} \overline{r_{12}} & \overline{t_{21}} \\ \overline{t_{12}} & \overline{r_{21}} \end{bmatrix} = \begin{bmatrix} S_{11} & S_{12} \\ S_{21} & S_{22} \end{bmatrix} = \frac{1}{(k_m+1)Z_m + k_m Z_0} \times \begin{bmatrix} (k_m-1)Z_m - k_m Z_0 & 2\sqrt{k_m} Z_m \\ 2\sqrt{k_m} Z_m & (1-k_m)Z_m - k_m Z_0 \end{bmatrix}. \quad (5)$$

The reflection and transmission coefficients obtained from Eq. (5) can subsequently be substituted into Eq. (1) to calculate the overall reflection, as well as the absorption. The absorption diagrams calculated by using parameters retrieved from transmission line model and full-wave electromagnetic simulations for different spacer thicknesses are plotted in Figs. 4(a) and 4(b). The marked similarity between the theoretical and numerical results validates the transmission line modeling. The absorption peak amplitude gradually increases as the spacer becomes thicker until the critical spacer thickness, beyond which the absorption peak amplitude decreases.

B. Conditions for perfect absorption

Finally, our approach allows for the determination of analytical expressions (see derivation presented in the Supplemental Material [23]) of the critical spacer thickness (d_p) and the corresponding frequency (f_p) for perfect absorption, which are expressed as

$$d_p = \frac{k_c \cdot (k_m+1) \cdot c}{4\pi f_{\mathrm{LC}}} \sqrt{\frac{a}{Z_0} - \frac{a^2}{Z_0^2}}, \quad (6)$$

$$f_p = f_{\mathrm{LC}} - \frac{\sqrt{aZ_0 - a^2}}{4\pi L_{\mathrm{LC}}}, \quad (7)$$

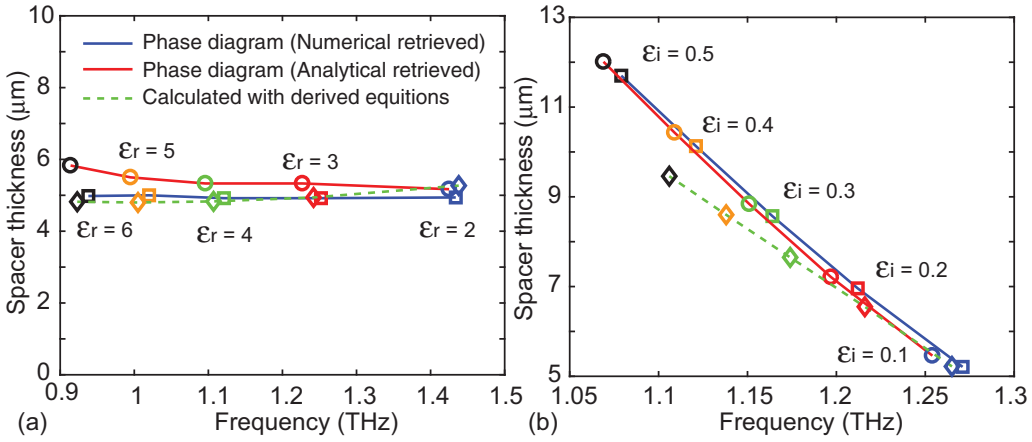

FIG. 5. Perfect absorption frequencies determined from simulations, analytical calculations based on Eqs. (1)–(5), and the explicit values from Eqs. (6)–(8). The lines are to guide the eye. (a) Varying ε_r while keeping $\varepsilon_i = 0.0843$. (b) Varying ε_i while keeping $\varepsilon_r = 2.81$.

where k_c is a correction coefficient chosen as 1.4 for our case (see further details in the Supplemental Material [23]), c is the speed of light in vacuum, a is the real part of Z_m composed of the metallic loss of the metamaterial structure [first term on the right side of Eq. (2)] and the dielectric loss of the spacer material [second term on the right side of Eq. (2)], and f_{LC} is the LC resonant frequency for the MMs on polyimide (in the absence of a ground plane):

$$f_{\mathrm{LC}} = \frac{1}{2\pi}\sqrt{\frac{2}{L_{\mathrm{LC}}C_{\mathrm{LC}}(\varepsilon_{\mathrm{r}}+1)}}. \tag{8}$$

C. Spacer permittivity and perfect absorption

The predictions from Eqs. (6)–(8) can be compared to the values obtained from full-wave electromagnetic simulations [e.g., phase shift diagrams like that in Fig. 2(d)] and from the analytical calculations using Eqs. (1)–(5). This comparison is made in Figs. 5(a) and 5(b) for different combinations of spacer material permittivity. The results for the three approaches are calculated at discrete points (as described below) and the lines are to guide the eye. In Fig. 5(a), the imaginary permittivity (ε_i) was kept constant (0.0843), while the real part (ε_r) increases from 2 to 6. With increasing ε_r, the resonant frequency of the MMs decreases due to the increased equivalent capacitance [Eq. (2)] and, thus, according to Eq. (7), the absorption peak frequency undergoes a red shift. However, the critical spacer thickness for perfect absorption remains nearly constant since the SRR resonant frequency (f_{LC}) and the loss of the system (a) decrease at the same time, essentially canceling one another [see Eq. (6)]. In Fig. 5(b), the real permittivity is held constant (2.81), while ε_i increases from 0.1 to 0.5. Due to the increase in the loss caused by the larger ε_i, the spacer thickness for perfect absorption increases [according to Eq. (6)], and the frequency undergoes a redshift [according to Eq. (7)]. Clearly, Eqs. (6)–(8) agree quite well with the numerical simulations and the calculations using Eqs. (1)–(5), although the discrepancy increases with larger loss [Fig. 5(b)] due to the low loss assumption in the derivation of Eqs. (6)–(8). With the retrieved spacer thickness, one can optimize the design to realize perfect absorption. Figure S3 [23] shows the absorption spectra with the optimized spacer thicknesses for different permittivity combinations. It is worthwhile to note the importance of the loss for the occurrence of the perfect absorption. As shown in Eq. (6), when the loss is zero ($a = 0$), the critical spacer thickness must be zero, which essentially means no perfect absorption for any spacer layer thickness.

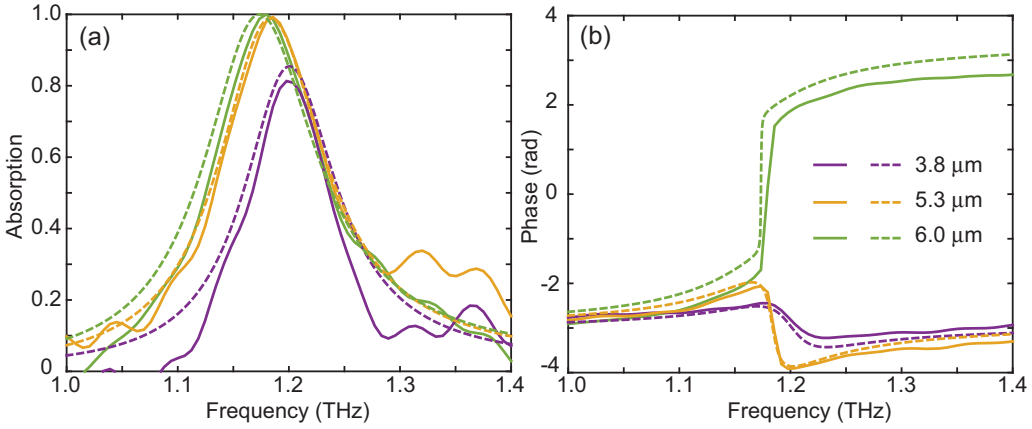

FIG. 6. Experiment (solid lines) and simulation (dashed lines). (a) Absorption spectra and (b) total reflection phase spectra for treated metamaterial absorbers with different spacer thicknesses. Results should be compared to Fig. 3.

D. Experimental verification

The dramatic increase in the phase shift in the vicinity of the critical spacer thickness was experimentally verified in Fig. 3(b). We have used these same samples to investigate the effects of increased loss due to an increase in ε_i of the dielectric spacer layer. This was accomplished by exposing the perfect absorbers to 85% humidity for 48 h at 40°C resulting in water absorption, which increases the loss of the polyimide spacer [26]. THz-TDS was used to characterize the samples right after the treatment. We estimate that the dielectric response of the polyimide changes from $2.81 + i0.084$ to $2.9 + i0.1305$—that is, the permittivity increases as does the loss with increasing humidity. The measured absorption spectra and reflection phase spectra are plotted in Fig. 6 with solid lines, and the simulation results are depicted in Fig. 6 with dashed lines. By comparing with Figs. 3(a) and 6(a), it is clear that the increase in the real part of the permittivity of the spacer material (from 2.81 to 2.90) causes the red shift of the absorption peaks. More interestingly, comparing Figs. 3(b) with 6(b) reveals that as the loss in the spacer material increases (from 0.0843 to 0.1305), the critical spacer thickness increases from 5.3 to 6.0 μm. This is evident because the phase shift spectra for the 5.3-μm film no longer exhibits a full 2π phase shift following water absorption by the polyimide, indicating that this is below the critical spacer layer thickness required for near-unity absorption.

IV. DISCUSSION AND CONCLUSION

Our theoretical and experimental results demonstrate that the perfect absorption frequency of metamaterial absorbers is closely related to the bare resonant frequency of the SRR array and is determined by the metallic structure of the SRRs ($L_{\mathrm{LC,dipole}}$ and $C_{\mathrm{LC,dipole}}$) and by the permittivity of the spacer material (ε_r). The frequency shifts are governed by the material loss stemming from both the metallic loss of the metamaterial structure ($R_{\mathrm{LC,dipole}}$) and the dielectric loss of the spacer material (ε_i). More specifically, an increase in ε_r redshifts the absorption peak frequency, and with higher material loss, a larger spacer thickness is needed for perfect absorption. The frequency and the spacer thickness can be accurately identified on the phase diagram as shown in Fig. 2(d) or approximately calculated with Eqs. (6) and (7).

In conclusion, we demonstrate that the perfect absorption frequency and spacer layer thickness can be visually pinpointed on plot of the phase shift of the total reflection. Additionally, using the transmission line theory to model the metamaterial resonators, we have obtained analytical formulas for the perfect absorption frequency and spacer layer thickness that reveal the functional dependence on material losses. We note that our findings are not directly applicable to absorbers with other configurations, such as all metal or all dielectric absorbers [27,28]. Nonetheless, our findings offer a powerful tool for the design and optimization of metamaterial absorbers with a metamaterial—dielectric spacer—metal configuration. Our results can be reasonably scaled across the spectrum.

ACKNOWLEDGMENTS

We acknowledge the National Science Foundation under Grant No. EECS-1309835 and the Army Research Office under ARO W911NF-16-1-0361. The authors thank Boston University Photonics Center for technical support. The authors thank Dr. Kaori Fukunaga for suggesting to utilize water absorption in polyimide to increase the dielectric loss.

[1] N. I. Landy, S. Sajuyigbe, J. J. Mock, D. R. Smith, and W. J. Padilla, Phys. Rev. Lett. **100**, 207402 (2008).
[2] H. Tao, N. I. Landy, C. M. Bingham, X. Zhang, R. D. Averitt, and W. J. Padilla, Opt. Express **16**, 7181 (2008).
[3] X. Liu, T. Starr, A. F. Starr, and W. J. Padilla, Phys. Rev. Lett. **104**, 207403 (2010).
[4] T. V. Teperik, F. J. Garcia de Abajo, A. G. Borisov, M. Abdelsalam, P. N. Bartlett, Y. Sugawara, and J. J. Baumberg, Nat. Photonics **2**, 299 (2008).
[5] B. A. Munk, P. Munk, and K. Pryor, IEEE Trans. Antennas Propag. **55**, 186 (2007).
[6] F. Costa, A. Monorchio, and G. Manara, IEEE Trans. Antennas Propag. **58**, 1551 (2010).
[7] E. F. Knott, J. F. Shaeffer, and M. T. Tuley, *Radar Cross Section*, 2nd ed. (Scitech, Raleigh, NC, 2004), pp. 327–334.
[8] D. T. Viet, N. T. Hien, P. V. Tuong, N. Q. Minh, P. T. Trang, L. N. Le, Y. P. Lee, and V. D. Lam, Optical Communications **322**, 209 (2014).
[9] X. Zhao, J. Zhang, K. Fan, G. Duan, G. D. Metcalfe, M. Wraback, X. Zhang, and R. D. Averitt, Photonics Res. **4**, A16 (2016).
[10] J. Grant, Y. Ma, S. Saha, A. Khalid, and D. R. S. Cumming, Opt. Lett. **36**, 3476 (2011).
[11] X. Zhao, K. Fan, J. Zhang, G. R. Keiser, G. Duan, R. D. Averitt, and X. Zhang, Microsyst. Nanoeng. **2**, 16025 (2016).
[12] A. K. Azad, W. J. M. Kort-Kamp, M. Sykora, N. R. Weisse-Bernstein, T. S. Luk, A. J. Taylor, D. A. R. Dalvit, and H.-T. Chen, Sci. Rep. **6**, 20347 (2016).
[13] H.-T. Chen, J. Zhou, J. F. O'Hara, F. Chen, A. K. Azad, and A. J. Taylor, Phys. Rev. Lett. **105**, 073901 (2010).
[14] Q. Y. Wen, Y. S. Xie, H. W. Zhang, Q. H. Yang, Y. X. Li, and Y. L. Liu, Opt. Express **17**, 20256 (2009).
[15] A. Sellier, T. V. Teperik, and A. Lustrac, Opt. Express **21**, A997 (2013).
[16] J. Zhou, H.-T. Chen, T. Koschny, A. K. Azad, A. J. Taylor, C. M. Soukoulis, and J. F. O'Hara, arXiv:1111.0343.
[17] R. Alaee, M. Farhat, C. Rockstuhl, and F. Lederer, Opt. Express **20**, 28017 (2012).
[18] C. Qu, S. Ma, J. Hao, M. Qiu, X. Li, S. Xiao, Z. Miao, N. Dai, Q. He, S. Sun, and L. Zhou, Phys. Rev. Lett. **115**, 235503 (2015).
[19] H.-T. Chen, Opt. Express **20**, 7165 (2012).
[20] L. Huang, D. R. Chowdhury, S. Ramani, M. T. Reiten, S.-N. Luo, A. K. Azad, A. J. Taylor, and H.-T. Chen, Appl. Phys. Lett. **101**, 101102 (2012).
[21] A. K. Azad, A. J. Taylor, E. Smirnova, and J. F. O'Hara, Appl. Phys. Lett. **92**, 011119 (2008).
[22] F. Costa and A. Monorchio, IEEE Trans. Antennas Propag. **60**, 4650 (2012).

[23] See Supplemental Material at http://link.aps.org/supplemental/10.1103/PhysRevB.97.035128 for details of the fitting to obtain the effective circuit parameters, detailed derivation of equations for perfect absorption, and simulated perfect absorption spectra for the absorbers with optimal spacer thickness in Fig. 5.

[24] E. C. Burdette, F. L. Cain, and J. Seals, IEEE Trans. Micro. Theory Tech. **28**, 414 (1980).

[25] D. A. Frickey, IEEE Trans. Micro. Tech. **42**, 205 (1994).

[26] K. Fukunage and S. Kurahashi, IEEJ Trans. Electric. Electron. Eng. **2**, 596 (2007).

[27] M. Wu, X. Zhao, J. Zhang, J. Schalch, G. Duan, K. Cremin, R. D. Averitt, and X. Zhang, Appl. Phys. Lett. **111**, 051101 (2017).

[28] K. Fan, J. Y. Suen, X. Liu, and W. J. Padilla, Optica **4**, 601 (2017).